J Biomol NMR (2012) 53:71–83
DOI 10.1007/s10858-012-9620-y

ARTICLE

Thermal stability of chicken brain α-spectrin repeat 17: a spectroscopic study

Annette K. Brenner · Bruno Kieffer · Gilles Travé · Nils Åge Frøystein · Arnt J. Raae

Received: 17 November 2011 / Accepted: 12 March 2012 / Published online: 9 May 2012

Abstract Spectrin is a rod-like multi-modular protein that is mainly composed of triple-helical repeats. These repeats show very similar 3D-structures but variable conformational and thermodynamical stabilities, which may be of great importance for the flexibility and dynamic behaviour of spectrin in the cell. For instance, repeat 17 (R17) of the chicken brain spectrin α-chain is four times less stable than neighbouring repeat 16 (R16) in terms of ΔG. The structure of spectrin repeats has mainly been investigated by X-ray crystallography, but the structures of a few repeats, e.g. R16, have also been determined by NMR spectroscopy. Here, we undertook a detailed characterization of the neighbouring R17 by NMR spectroscopy. We assigned most backbone resonances and observed NOE restraints, relaxation values and coupling constants that all indicated that the fold of R17 is highly similar to that of R16, in agreement with previous X-ray analysis of a tandem repeat of the two domains. However, ^{15}N heteronuclear NMR spectra measured at different temperatures revealed particular features of the R17 domain that might contribute to its lower stability. Conformational exchange appeared to alter the linker connecting R17 to R16 as well as the BC-loop in close proximity. In addition, heat-induced splitting was observed for backbone resonances of a few spatially related residues including V99 of helix C, which in R16 is replaced by the larger hydrophobic tryptophan residue that is relatively conserved among other spectrin repeats. These data support the view that the substitution of tryptophan by valine at this position may contribute to the lower stability of R17.

Keywords Spectrin repeats · Dynamics · Stability · Conformation · Heteronuclear NMR spectroscopy

Electronic supplementary material The online version of this article (doi:10.1007/s10858-012-9620-y) contains supplementary material, which is available to authorized users.

A. K. Brenner · N. Å. Frøystein
Department of Chemistry, University of Bergen, PObox 7800, 5020 Bergen, Norway

B. Kieffer
IGBMC Biomolecular NMR Group, CNRS UMR 7104, Ecole Supérieure de Biotechnologie de Strasbourg, Boulevard Sebastien Brant BP10413, 67412 Illkirch Graffenstaden, France

G. Travé
Equipe Oncoproteines, IREBS, UMR 7242, Ecole Supérieure de Biotechnologie de Strasbourg, Boulevard Sebastien Brant BP10413, 67412 Illkirch Graffenstaden, France

A. J. Raae (✉)
Department of Molecular Biology, University of Bergen, PObox 7800, 5020 Bergen, Norway
e-mail: arnt.raae@mbi.uib.no

Introduction

Spectrin (Fig. 1a) is a key component in the regulation of dynamics and the shape of most vertebrate, as well as some metazoan cells (Bennett and Gilligan 1993). The protein is often described as a rod-like molecule consisting of two α (280 kDa) (Sahr et al. 1990) and two β (246 kDa) (Winkelmann et al. 1990) homologous chains that are associated and linked together to form the mature tetramer with actin binding motifs in both ends (Bennett and Gilligan 1993). Initial results from NMR spectroscopy on erythroid spectrins indicated that the proteins are more loosely packed than it appears from X-ray crystallography (Fung et al. 1986, 1989). Approximately 90 % of the spectrin molecule is made up of the so-called spectrin

repeats: usually 20 in the α-chain and 17 in the β-chain (Bennett and Gilligan 1993).

The general structure of a spectrin repeat is a left-handed coiled coil of three right-handed antiparallel helices (Pascual et al. 1996; Pascual et al. 1997), each consisting of approximately 106 amino acids (Fig. 1b). The helices are linked with two loops, whereas the repeats themselves are connected by a short linker region (Grum et al. 1999). Even though the repeated sequences show less sequence similarity than in other protein superfamilies, they consistently are made up of a repeating heptad pattern, the structural motif typical of coiled coils, where the positions are commonly denoted *a* through *g*. The *a* and *d* positions are occupied by non-polar residues that are involved in interhelical, hydrophobic interactions. The *e* and *g* positions often contain charged residues that can form interhelical salt-bridges with oppositely charged residues (Parry et al. 1992).

Chicken brain α-spectrin repeat 17 is a thoroughly studied domain. However, its thermal stability and its dynamics have not been analyzed by NMR spectroscopy. Indeed, only few structural solution analyses have been carried out so far on repeats belonging to the spectrin (Park et al. 2003; Pascual et al. 1997) and the α-actinin family (Kowalski et al. 2004), respectively. In this paper, a solution NMR study of R17 is presented.

The thermodynamical and conformational stabilities of mature spectrins are strongly associated with the functionality of the cell (An et al. 2006); however, the melting points for the different repeats within spectrin may vary with more than 50 K (An et al. 2006). The melting points for the neighbouring repeats 16 and 17 differ with 18 K and, in

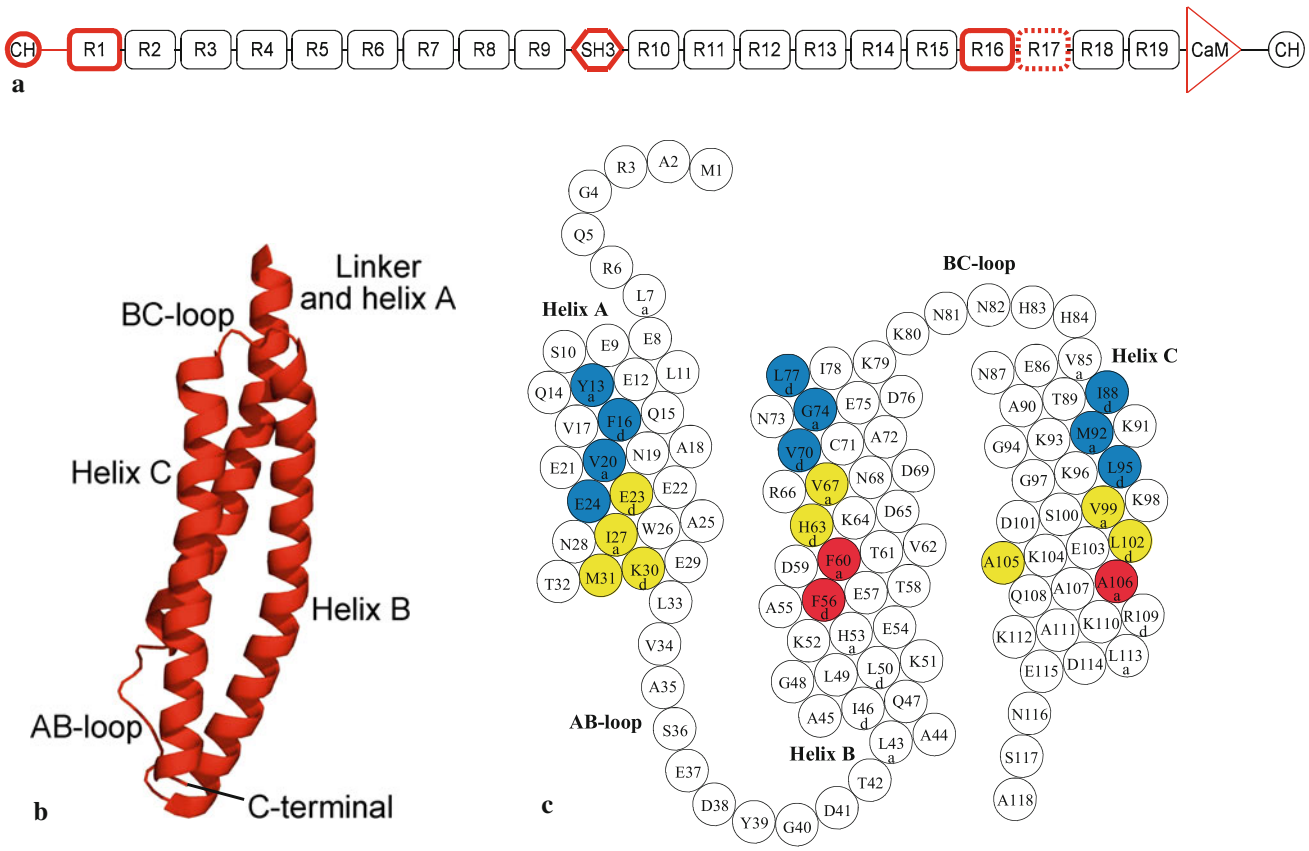

Fig. 1 Visualization of a spectrin chain and the chicken brain α-spectrin repeat 17. **a** A schematic view of a typical multi-modular spectrin molecule, including the spectrin repeats (annotated R1-R19). The modules that have been analysed by NMR-spectroscopy are marked in *red*: The actin-binding calponin homology (CH) domain (Carugo et al. 1997), R1 (Park et al. 2003), the src-homology 3 (SH3) domain (Musacchio et al. 1992), R16 (Pascual et al. 1996) and parts of the the calmodulin-like (CaM) domain (Travé et al. 1995). **b** Tertiary structure of our R17 construct according to the pdb-entry 1U4Q (Kusunoki et al. 2004b). Note that the construct includes parts of helix C of R16. The structure was displayed with the PyMOL Molecular Graphics System, Version 1.3, Schrödinger, LLC. **c** Schematic view of the triple-helix bundle of our R17 construct as observed by NMR-spectroscopy. The amino acids that face the hydrophobic core of R17 are indicated with the letters *a* and *d* beneath their residual labels. The colouring refers to groups of amino acids that show inter-helical NOE contacts to other residues highlighted with the same colour, e.g. V67 establishes long-range NOEs to both E23 and V99

terms of ΔG, R16 is four times more stable than R17 (Kusunoki et al. 2004b). It has recently been shown that two point mutations surrounding a *d* position in human dystrophin repeat 23, another member of the spectrin superfamily, are the main cause of a pathologic destabilization of helix C which results in muscular dystrophy (Legardinier et al. 2009). Thus, even small differences in the primary structure can have effect on the stability of a repeat.

In order to investigate the dynamics of the unfolding of R17, we undertook a detailed NMR analysis of this repeat including backbone assignment, measurements of ^{15}N-relaxation and H^N-exchange, and temperature dependent ^{1}H–^{15}N correlation spectra allowing to follow the evolution of individual residues of the domain upon heating. These data, together with sequence alignments, suggest that one cause of the reduced thermodynamical stability in R17 may be a destabilization in the centre of helix C, including the small hydrophobic valine (V99) that has substituted a tryptophan in R16.

Materials and methods

Construct preparation

Full-length cDNA from chicken brain α-spectrin was purchased from Seegene, Seoul, Republic of Korea. The pETM12 vector was a generous gift from G. Stier, University of Heidelberg.

Initially, a region from position 4309 to 6274 in the chicken brain α-spectrin gene that contains both R16 and R17 was amplified by PCR using 10 ng of the cDNA template. The forward and reverse primers were 5′-GCG TCT GAT CCA GTC ACA TC-3′ and 5′-CCT TTC TGA AGT GCT CCT GAG-3′, respectively. The primers were constructed to accommodate an *Nco*I restriction site in the 5′ end and an *Acc65*I site in the 3′ end. R17 was amplified by 5′-CCA TGC CAT GGC TCG GGG GCA ACG TCT GGA G-3′ as a forward primer and 5′- ATT GGT ACC TAC TAA TCT GCT TTC CAG TTG AAC-3′ as a reverse primer.

The gene was then ligated into the pETM12 vector. This vector contains a His-tag followed by a TEV recognition site at the N-terminus before the start of the expressed protein product.

Expression and purification of ^{13}C- and ^{15}N-labelled protein for NMR

Competent *E. coli* BL21 (DE3) cells were transformed by electroporation and cultured in 15 ml LB medium overnight at 37 °C and 250 rpm. The cell culture was then used to inoculate 150 ml M9 minimal medium with a LB to M9 medium ratio of 1:10.

The bacteria were grown until A_{600} was approximately 0.6. Recombinant protein expression was initiated with 0.4 mM IPTG upon incubation overnight at 18 °C. After pelleting, the bacterial cells were suspended in 30 mM imidazole, 1 mM β-mercaptoethanol and a cocktail of protease inhibitors (MERCK) in PBS pH 7.4 on ice. A cleared lysate was prepared after sonication and centrifugation at 20,000×*g* for 30 min at 4 °C. The lysate was then loaded on a Ni–NTA column equilibrated with 1 × PBS pH 7.4, 0.5 M NaCl, 30 mM imidazole, 1 mM β-mercaptoethanol and protease inhibitors. The His-tagged recombinant protein was eluted with the same buffer containing 230 mM imidazole. After concentration, the protein was further purified on a Superdex 75 column using FPLC with 1 × PBS buffer, pH 7.4, including 0.2 M NaCl and 1 mM DTT. The His-tag was removed by enzymatic digestion of R17 with TEV-protease. Pure R17 was yielded from a Ni–NTA column equilibrated with NMR buffer, consisting of 20 mM sodium phosphate buffer pH 6.8, 0.1 M NaCl, 1 mM DTT and 0.05 % NaN_3.

NMR Spectroscopy

Unless otherwise stated, approximately 200 µM purified R17 (600 µl, ^{13}C and ^{15}N labelled) dissolved in NMR buffer (containing 10 % D_2O) was used in the NMR experiments.

The spectra were collected at 600.13 MHz (^{1}H) on a Bruker Biospin AV600 spectrometer equipped with a superconducting actively shielded magnet. A 5 mm triple resonance (^{1}H, ^{13}C, ^{15}N) inverse cryogenic probehead with z-gradient coils and cold ^{1}H and ^{13}C pre-amplifiers was used. All 3D experiments were conducted at 298 K. The spectra were processed using Bruker Biospin's TopSpin 1.3 software. Cara was used for resonance assignment (Keller 2005). The NOESY-spectra were analysed using CcpNmr Analysis (Vranken et al. 2005). The ^{1}H and ^{13}C chemical shifts were referenced to DSS as internal standard. The ^{15}N chemical shifts were calculated from the adjusted ^{1}H frequency (Harris et al. 2008). In spectra without DSS, the signal of the solvent HDO was set to 4.76 ppm as this was the measured shift value of HDO in the DSS-sample. Furthermore, 4.76 ppm is the calculated shift for HDO at this temperature, pH and ionic strength (Wishart et al. 1995). Important acquisition parameters for all conducted experiments are listed in Table S1.

Backbone and side chain assignment

The amide ^{1}H and ^{15}N resonances of the protein were obtained using the 2D ^{1}H–^{15}N HSQC experiment (Grzesiek and Bax 1993b; Davis et al. 1992).

Sequential backbone assignment was achieved using standard 3D triple resonance experiments (Sattler et al.

1999). For further diminishing of side chain ambiguity and better distinguishing of overlapping residues (Fig. S1), 3D CC(CO)NH (Montelione et al. 1992; Grzesiek et al. 1993) with an isotropic mixing time of 28 ms and several amino acid edited 2D ^{1}H–^{15}N HSQC, or MUSIC (Schubert et al. 2001a, b; Schubert et al. 1999), spectra were recorded.

Side chain ^{1}H-shifts were obtained from HBHA(CO)NH (Grzesiek and Bax 1993a) and H(CC)(CO)NH (Grzesiek et al. 1993; Montelione et al. 1992) experiments, using an isotropic mixing time of 35 ms in the latter experiment. Most of the H^{δ} and H^{ε} chemical shifts of phenylalanine and tyrosine could be determined from the 2D (HB)CB(CGCD)HD and (HB)CB(CGCDCE)HE experiments (Yamazaki et al. 1993).

NOE restraints and coupling constants

3D ^{1}H–^{13}C HSQC-NOESY ^{1}H–^{15}N HSQC (CN-NOESY) (Diercks et al. 1999), 3D ^{15}N NOESY-HSQC and 3D ^{13}C NOESY-HSQC (Davis et al. 1992) spectra, all with a mixing time of 120 or 125 ms, were acquired in order to determine the secondary structure of R17 and to verify the presence of the triple-helix bundle.

The ^{3}J (H^{N}–H^{α}) coupling constants over the dihedral Φ-angles were estimated from the HNCA E.COSY spectrum (Weisemann et al. 1994).

Protein dynamics experiments

^{15}N T_1 and T_2 relaxation times and ^{15}N–{^{1}H} heteronuclear NOEs (hetNOE) were measured using 2D ^{1}H–^{15}N HSQC based methods (Kay et al. 1989). All spectra were recorded with 2048 complex data points for each of 128 t_1 increments with 8 scans per t_1 point, except for hetNOE where 16 scans were gathered for each of 256 t_1 increments.

T_1 values were obtained using three parallel series of following ten randomized relaxation delays: 50, 210, 370, 530, 690, 850, 1010, 1170, 1330 and 1490 ms. T_2 values were recorded in three parallel series of nine randomized relaxation delays: 0, 17.6, 35.2, 52.8, 70.4, 88, 105.6, 123.2 and 140.8 ms. Finally, four interleaved hetNOE spectra were recorded. In the spectra with NOE a proton saturation time of 3 s and a recycling delay of 9 s were used, whereas in the spectra without NOE the recycling delay was 12 s. No saturation was included in the latter case.

All spectra were processed with the NMRPipe software package (Delaglio et al. 1995) using Gaussian window functions in both frequency domains. Peak heights were measured in all spectra of a relaxation series and fitted with a two-parameter single-exponential function to extract the relaxation rates, except for the hetNOE experiments, where the result is determined by the intensity ratio from the spectrum with NOE and the reference spectrum without NOE, averaged for the four experiments. From the repeated determination of the relaxation parameters and statistical Monte-Carlo simulations (Kamath and Shriver 1989) in NMRPipe, an estimated relative error of 7 % for all residues was introduced.

H^{N}-exchange

In order to detect backbone-NH signals that were solvent-exchanged at our regular conditions, a 2D ^{1}H–^{15}N HSQC spectrum was collected on approximately 150 μM R17 at pH 6.0 instead of 6.8 for comparison with earlier reported R16 acquisition data.

In addition, 100 µl of this sample was dissolved in 500 µl D_2O and the exchange of the backbone-NH resonances at 296 K was monitored over 72 h with a total of ten 2D ^{1}H–^{15}N SOFAST-HMQC experiments (Schanda et al. 2005). Approximate exchange time constants were calculated from the peak heights in the spectra fitted to a two-parameter single-exponential function which decays to a constant relative intensity (16.7 %). A three-parameter fit did not yield any better results mainly due to low spectral sensitivity.

Thermal protein denaturation

In order to identify labile amino acids that might indicate the region of R17 where protein unfolding initially occurs, approximately 50 µM of the protein (pH 6.0) was heated with small temperature increments of 0.5 or 1.0 K until just below its melting point. 2D ^{1}H–^{15}N SOFAST-HMQC spectra were recorded in the 298–321 K range.

Furthermore, 3D HNCO and HN(CO)CA experiments at 317 K were conducted on the 200 µM sample (pH 6.8) in order to look for reduced helicity from the C' and C^{α} chemical shift indices.

The melting points of R17 and the double repeat R1617 were determined by circular dichroism (CD). Both measurements were performed on 5 µM protein in 250 µl PBS, pH 7.4, in a Jasco J-810 spectropolarimeter equipped with a Jasco PTC-423S Peltier element for temperature control. The changes in ellipticity at 222 nm were monitored with a scan-rate of 1 K/min in the 293–343 K range.

Results

NMR assignment

Approximately 92 % of all ^{1}H, ^{13}C and ^{15}N chemical shifts in R17 were assigned (BMRB-accession: 18260) using 3D heteronuclear NMR experiments in combination with amino acid edited ^{1}H–^{15}N HSQC spectra. A total of eight

backbone-NH correlations are not observed at the reported conditions. The missing shifts belong, with one exception, to amino acids positioned in the linker and the BC-loop.

Secondary structure and triple-helix bundle

The positions of the secondary structural elements of R17 were determined by the chemical shift deviations of the C^{α}, C^{β}, C' and H^{α} shifts compared to their random coil values (Wishart et al. 1995; Wishart et al. 1991), the patterns of sequential and medium-range NOESY-signals (Wüthrich et al. 1984), and estimates of backbone ^{3}J (H^{N}–H^{α}) coupling constants (Vuister and Bax 1993). The C^{α} chemical shift deviations, which are the best indicator for determining helical structures (Wang and Jardetzky 2002), and the secondary structure chart are shown in Fig. 2. According to the results, helices A (including most of the linker, ^{7}LEESLE^{12}), B and C encompass residues 8–33, 43–79, and 86–115 of the construct, respectively. While the first six residues of the construct normally form part of helix C in R16 (pdb-entry 1CUN), in isolated R17 these residues are not fully folded. However, lower values of ^{3}J (H^{N}–H^{α}) coupling constants together with consistently small, biased values of C^{α} and C' chemical shifts indicate transient helical conformations. The chemical shift deviations of the other three nuclei, where especially the C' shifts are in very good agreement with the proposed helical positions, are presented in Fig. S2.

The presence of the triple-helix bundle typical of spectrins was confirmed by interhelical NOE-correlations detected by 3D ^{13}C NOESY-HSQC. Interhelical contacts were observed for seven residues in each of the three helices: Y13 (A4),[1] F16 (A7), V20 (A11), E23 (A14), E24 (A15), I27 (A18) and M31 (A22) in helix A, F56 (B11), F60 (B15), H63 (B18), V67 (B22), V70 (B25), G74 (B29) and L77 (B32) in helix B, and I88 (C4), M92 (C8), L95 (C11), V99 (C15), L102 (C18), A105 (C21) and A106 (C22) in helix C. The interhelical NOEs seemed to divide into three spatial segments within the helices. These are indicated by different colours in Fig. 1c. A detailed description of the long-range NOEs is listed in Table S2.

Relaxation

^{15}N–{^{1}H} heteronuclear relaxation was measured to probe both the local and global dynamics of the domain and further investigate the agreement between the solution structure of R17 and its previously published X-ray structures. The experimental T_1, T_2 and hetNOE values are plotted against the amino acid sequence in panels a, b and c of Fig. 3. The average values are 920 ms for T_1 and 63 ms for T_2, respectively. The profile of the hetNOE values (Fig. 3c) is in agreement with the proposed positions of the α-helices. Low hetNOE values (below 0.7) at both termini of the domain and within the AB-loop are consistent with the occurrence of high-frequency motions in these regions. However, the T_2-values of the N-terminal residues R6 and L7 show an increased helix propensity.

The average T_1/T_2 ratio of 14.6 is compatible with the overall tumbling time of a protein of 118 residues as indicated by a calculation of the diffusion tensor performed using the HydroNMR software (de la Torre et al. 2000) and the crystal structure (pdb-entry 1CUN). This calculation showed the highly anisotropic nature of the triple-helix bundle structure and predicted a factor of about 3 between axial and perpendicular rotational diffusion rates.

The relaxation rates were therefore analysed by a fully anisotropic model using TENSOR2 (Dosset et al. 2000). The rotational diffusion tensor was determined from the R_2/R_1 ratios of residues assumed to belong to rigid parts of the repeat using a two steps procedure. A first fit based on 82 residues was performed and led to a very good agreement between the main axis of the diffusion tensor and the smallest axis of the inertia tensor, a striking finding given the poor sampling of all possible N–H vector orientations due to the co-linear triple-helix geometry of R17. Since 17 residues displayed significant deviation from the model, a second fit was performed using a subset of 65 selected residues. The main axis of the resulting tensor was fully superposable with the one obtained from the first calculation with less than 2° difference between both axes. The resulting χ^2 value of 49.1 allowed to accept the hypothesis of an axially symmetric tensor with a confidence level of 0.05. No significant improvement was obtained by using a fully anisotropic tumbling model. Monte-Carlo simulations showed a very robust definition of the main axis of the diffusion tensor by relaxation data (Fig. 3e); an observation that was further confirmed using a "leave-one-out" procedure where 15 % of the data were randomly left out (data not shown). The eigenvalues of the diffusion tensor were $(2.86 \pm 0.14) \times 10^{7}$ and $(1.22 \pm 0.10) \times 10^{7}$ s^{-1} for the main and perpendicular axis respectively, resulting in a global correlation time, $\tau_{c,eff}$, of approximately 9.4 ± 0.2 ns.

The order parameter values, S^2 (Fig. 3d), were calculated by using a model for the Lipari-Szabo approach (Lipari and Szabo 1982a, b). The overall pattern of the S^2 values indicates that R17 is very rigid in solution.

Interestingly, the bend in helix B allows for a wider sampling of the N–H vector orientations than initially anticipated, explaining the larger dispersion of the relaxation times measured for the corresponding residues. Helix C, on the other hand, is nearly perfectly straight and parallel with the main rotational axis (Fig. 3e). As a result, all

[1] Amino acid numbering in parentheses is according to the nomenclature of Yan et al. (1993).

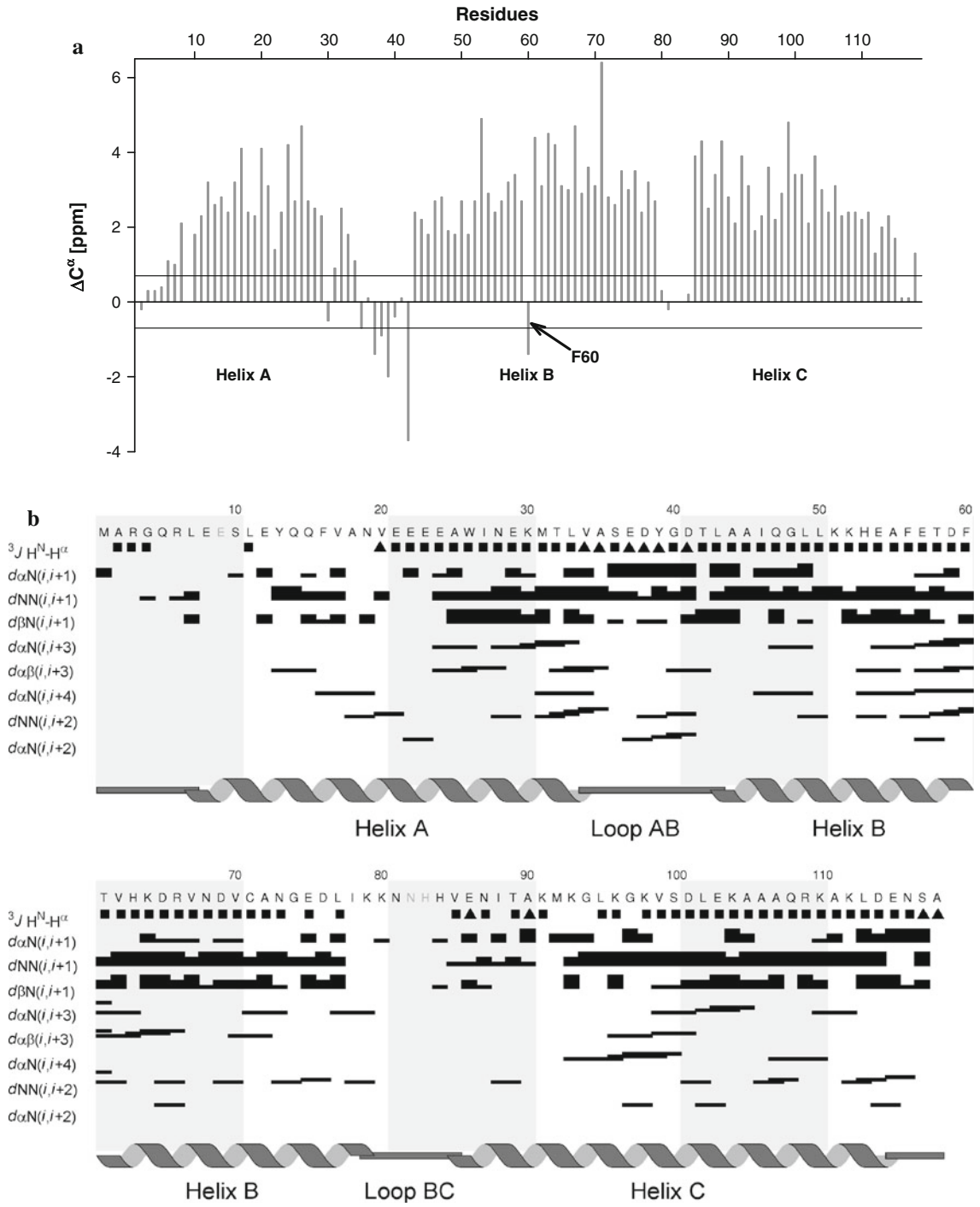

Fig. 2 The secondary structures of R17. **a** The C^{α} chemical shift deviations in ppm compared to the random coil values are plotted against the residual number. The values between the two *horizontal lines* in the plot indicate random coil values. Values above this deviation (0.7 ppm) are correlated with a helical position. The graph indicates three large helices (residues 8–33, 43–79 and 86–115). Deviations from the α-helical pattern, like the marked F60, might be explained by aromatic ring current effects. F60 is stacked on top of the aromatic ring of F56 as seen from the crystal structure (Grum et al. 1999), that could lead to an upfield shift of, among others, the C^{α} chemical shift. Chemical shifts for E9, N82 and H83 are missing. **b** Secondary structure chart of R17. The amino acid sequence and the residue numbers are given at the top. No information is available for residues in light gray, i.e. E9, N82 and H83. Solid squares represent a ^{3}J (H^{N}–H^{α}) coupling constant smaller than 6.0 Hz, indicating a helical structure, while solid triangles represent coupling constant larger than 6.0 Hz, indicating a loop or a strand. Sequential NOE-connectivities are indicated by bars, where the thickness of the bars illustrates the relative intensity of the NOE-crosspeaks. Medium-range NOE-connectivities are indicated by thin lines covering the length of the connected residues. Due to massive peak overlap in the 3D ^{15}N NOESY-HSQC experiment, many of the weaker medium-range NOESY-interactions, typical of α-helices, are not observable. The proposed locations of the helices and loops are shown at the bottom

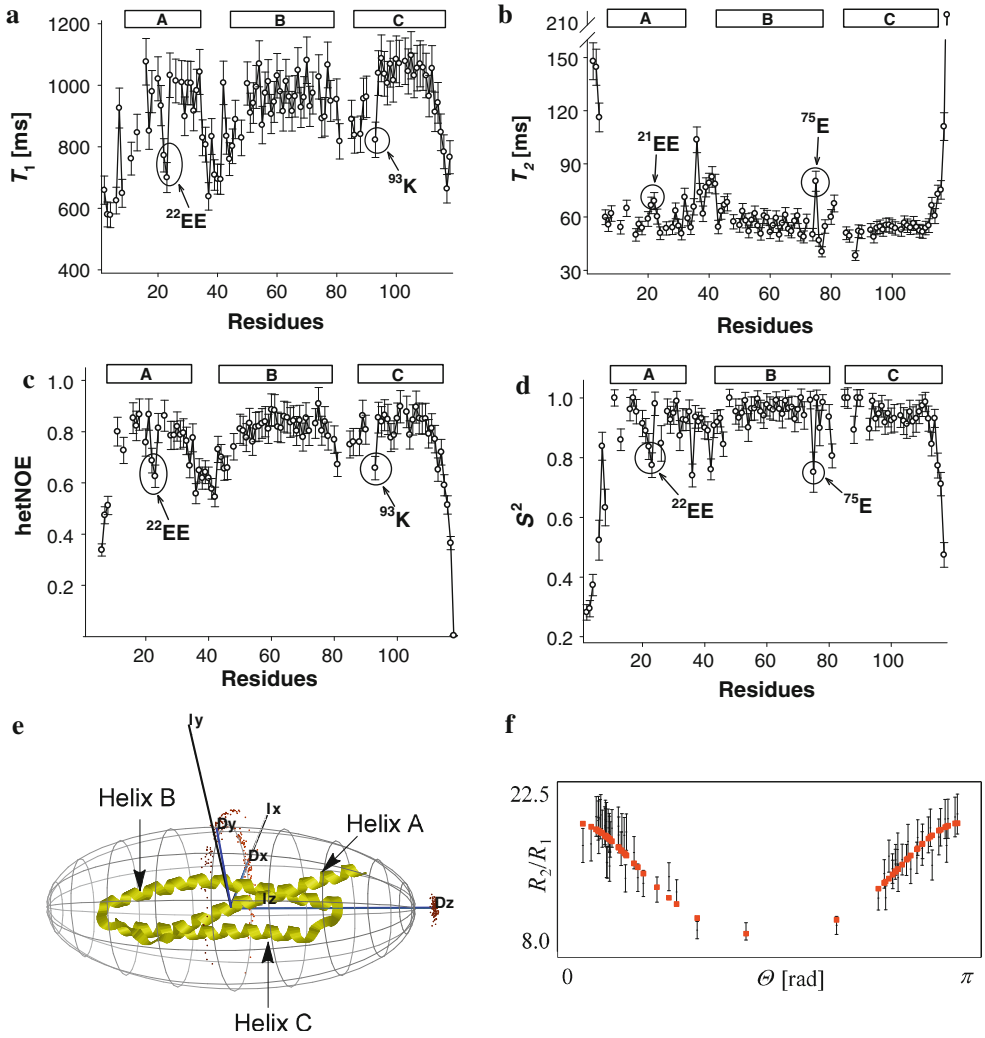

Fig. 3 **a**–**c** Relaxation data with estimated relative residual errors of 7 %. Missing residues are due to conformational exchange or severe overlap in the ^{1}H–^{15}N HSQC spectrum. The position of the helices and amino acids that show deviations from the helical values are indicated. **a**, **b** ^{15}N T_1 and T_2 values. The anisotropy of R17 can clearly be seen as the oscillation of the T_1 and T_2 times in helix B. **c** ^{15}N–{^{1}H} hetNOE ratios. Negative values for residues 2–4 were removed for clarity. **d** Calculated S^2 values with their standard deviations. **e** The axial symmetric rotational diffusion tensor components embedded in the molecular structure of R17. The dots represent diffusion tensor orientations obtained from a 100 step Monte-Carlo simulation. The model is visualized in TENSOR2 (Dosset et al. 2000). Note that the model is based upon the crystal structure of R1617 (pdb-entry 1CUN) (Grum et al. 1999) and that the first seven N-terminal amino acids in the single repeat are unstructured and not helical as indicated. **f** A plot of R_2/R_1 against Θ showing the similarity between the structural data from our NMR results and the X-ray structure

^{15}N–H relax at about the same rates and this helix shows no direct sign of anisotropic motion.

The comparison of the angles (Θ) between the principal axis of the helix-bundle and the N–H vectors obtained from R_2/R_1 ratios and the crystal structure led to a reasonable agreement (Fig. 3f and Table S3), supporting the assumption that the crystal structure of the domain is conserved in solution. However, some residues deviate considerably from the main trend. They are mostly found in the more flexible parts of the repeat, within or close to the loops (S36, D41, T42, L43, I46, E75-L77 and N81) and the first half of helix A (Y13, F16, A18, E22, E23 and W26).

Overall, the results from the chemical shift data, the coupling constants, the sequential and medium-range NOE connectivities and the different relaxation data are all in agreement with the secondary structures found in the crystal structure of the R1617 double repeat.

H^N-exchange

To further investigate the local differences in flexibility of the repeat, H^N-exchange experiments were performed. Approximately half of the backbone-NH correlations and all the side chain-NH signals were immediately deuterated

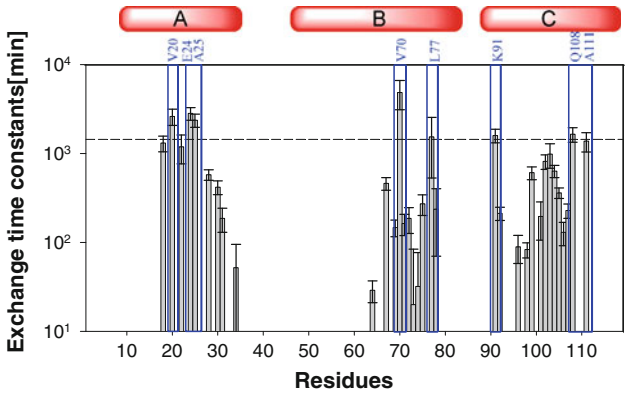

Fig. 4 H^N-exchange at 296 K. The exchange time constants (log scale) with their standard deviations are plotted against the residual number. Residues with exchange times above the *horizontal line* (24 h) are defined as very slow-exchanging. The helices and the identity of the very slow-exchanging amino acids are shown on top of the plot

after 84 % D_2O was added to the R17-sample. Regions displaying the fastest exchange rates were the N-and the C-termini, the loops, the entire first half of helix B (L43-F56) which in the single repeat is not stabilised by another helix and most of the solvent-exposed parts of helices A and C. Each helix contains a region where a majority of the amino acids are protected against immediate solvent-exchange: A18-A25 in helix A, V67-I78 in helix B and K96-A111 in helix C. Still, only eight residues were not solvent-exchanged within the first 24 h: V20, E24 and A25 in helix A, V70 and L77 in helix B and K91, Q108 and A111 in helix C (Fig. 4). Most of these residues are either located at or in the vicinity of the hydrophobic core between the three helices in the R17 triple-helix bundle.

Thermal stability

The melting temperature of the R17 construct obtained from CD analysis at 222 nm was about 313 K, and at temperatures above 320 K the protein was entirely denatured (Fig. 5a). The double repeat of R1617 (insert in Fig. 5a) shows the two-phased melting of the structure as R17 melts first at approximately 311 K followed by R16 at approximately 328 K. The figure highlights the stability difference between the two spectrin repeats.

In order to get insight into the thermal unfolding pathways at an amino acid level, the NMR sample was heated stepwise from 298 to 321 K and ^1H–^{15}N HMQC spectra were recorded at each step. Residues with the most extreme H^N-shifts moved closer to the centre of the spectrum indicating destabilization of the helices (Fig. 5d). At about 319 K the peak intensity decreased for most residues. Still, the protein was at no time irreversibly denatured as the HMQC-spectrum recorded immediately after a rapid cool-down back to 298 K was identical with the original spectrum.

In the range of 312–317 K, some signals split into two or more distinct peaks, where intensities built up at new resonance positions (Fig. 5b, c and e) indicating destabilization of the structure. The affected residues are positioned at the N- and C-termini (A2, G4 and A118) and the transition between loops and helices (K30, T32, V34, D41 and N87). In addition, peak splitting was observed for a total of six helical resonances: T58, A90, L95, G97, S100 and A111. The residues that were directly affected by temperature increments are marked with different colours in the primary structure of R17 (Fig. 5f). Most of these peaks remained split during further temperature increase while, for instance, G4 only split over a temperature-interval of seven degrees before the entire peak shifted to the new resonance position. The absolute changes of the H^N chemical shifts of 79 resolved NH-correlations are shown in Fig. S3. Surprisingly, also the C' and/or C^α chemical shifts of seven residues underwent peak splitting at 317 K: A25, L33, E57, F60, V70, G94 and V99 (chemical shift values are listed in Table S4). In some cases, the splitting of the NH-crosspeaks appeared to be correlated with a splitting of the C'/C^α signals of the preceding residue as observed for residues V34, T58, L95 and S100. Remarkably, the residues subject to peak splitting are localized within a central area of the domain, in particular V99 that forms a core structural triad together with W26 and F60 (Fig. 5f).

Discussion

This work was carried out in order to reveal the molecular basis for the different stabilities of the two neighbouring spectrin repeats 16 and 17. Our NOESY and relaxation data and the coupling constants indicated that the fold of R17 is highly similar to that of R16 and in agreement with X-ray data of these domains. By performing dynamic analysis, including the thermal stability study, we observed features of R17 that might contribute to explaining its lower stability when compared to R16. We observed heat-induced splitting for the backbone resonances of a few spatially close residues, suggesting that they are involved in the same collective process in the unfolding pathway. This area was located around the small hydrophobic V99 of helix C, which in R17 has replaced the relatively conserved tryptophan found at the same position in R16.

Conformational exchange in R17

While all backbone NH-correlations could be observed in R16 (Pascual et al. 1996), there are a total of eight missing NH-signals in R17: E9, S10, E12, N19, K79, N82, H83 and

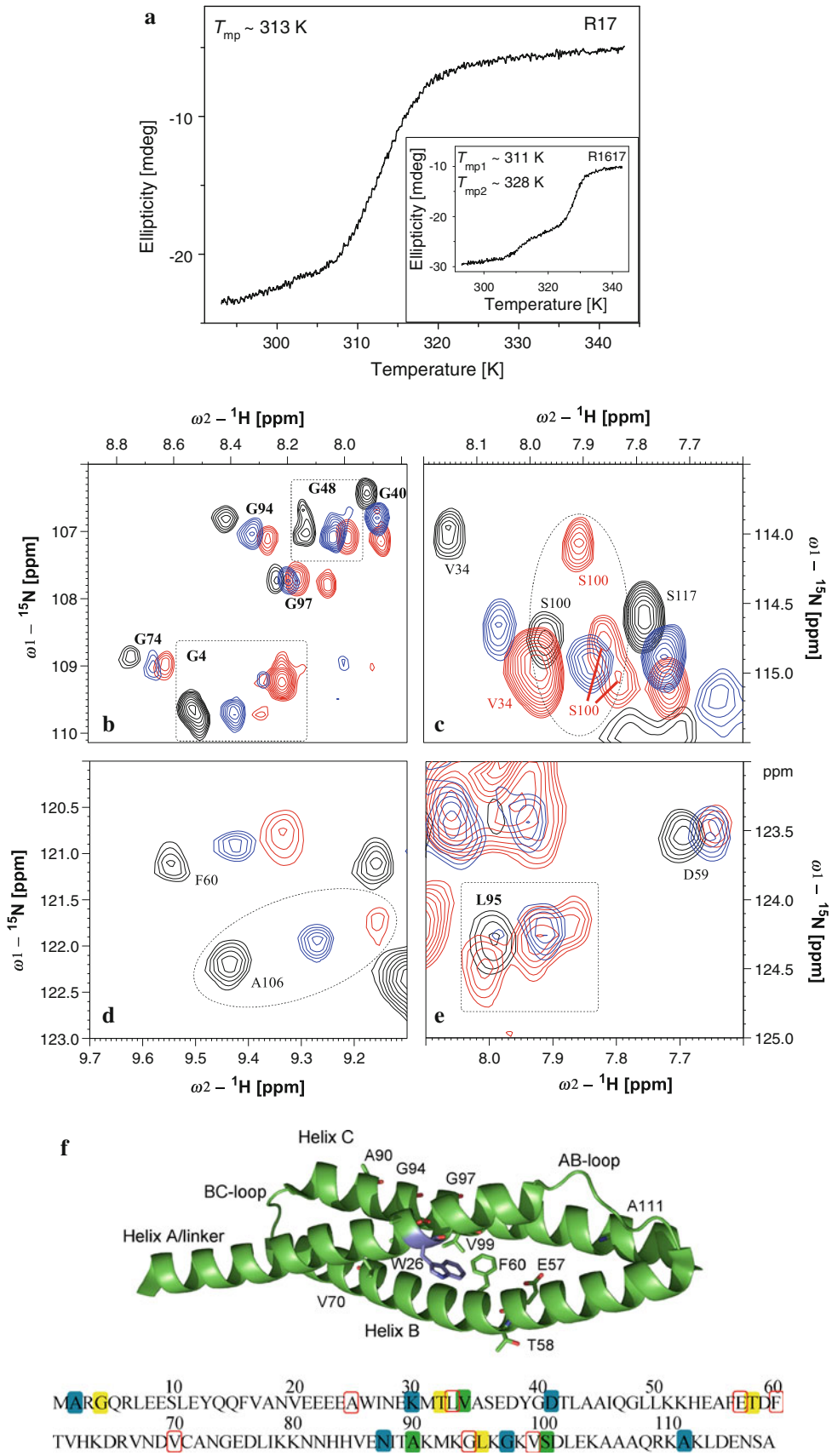

Fig. 5 Effect of temperature increase. **a** CD-melting curves of R17 and the double repeat R1617 (insert). The ellipticity at 222 nm is plotted against the temperature of the protein sample. The melting temperatures read from the plot are indicated. **b–e** Effect of temperature increment demonstrated on a selection of peaks in the $^{1}H–^{15}N$ HMQC-spectrum at three particular temperatures: 298 K (*black*), 313 K (*blue*) and 321 K (*red*). **b** The glycine region: G4 at the N-terminal is split into two distinct peaks at 313 K, while at 321 K (almost) the entire signal is shifted to the new position. G97 is split into two distinct peaks at 321 K. **c** S100 splits into three signals at temperatures above 320 K. **d** The two amino acids with the most extreme H^{N}-shifts at room temperature, F60 and A106, move closer to the centre of the spectrum as the temperature is raised. **e** L95 splits into three signals at temperatures above 315 K. **f** In the tertiary structure (pdb-entry 1CUN), helical residues that show splitting of their backbone-signals are indicated with sticks. W26 (*blue*) itself displays no splitting, but is shown because it is the most central amino acid in the hydrophobic core of R17. In the primary structure of R17, residues that are affected by temperature increments are highlighted with different colours. The colours indicate onset of changes at 310–312 K (*yellow*), approximately 315 K (*green*) and temperatures above 317 K (*blue*). Residues which are marked in *red* show peak splittings of their backbone carbons at 317 K

H84. Except for N19, these missing amino acids are either positioned in the linker or within the BC-loop. It should be noted that experiments conducted at the same pH-value as those of Pascual et al. (1996) and in the temperature range of 283–321 K did not restore any missing correlations. This suggests that the lack of signal may be rather due to conformational exchange processes than fast solvent exchange. The ^{1}H–^{15}N HSQC spectrum showed that the NH-signals of L7, L11, K80 and N81 are broadened, indicating that the residues close to amino acids that are missing from the spectrum are also involved in conformational exchange. Furthermore, short T_2 relaxation times observed for the C-terminal of helix B evidence exchange line broadening within the BC-loop region. E75, for instance, relaxes at the same rate as residues in the two loops (Fig. 3b).

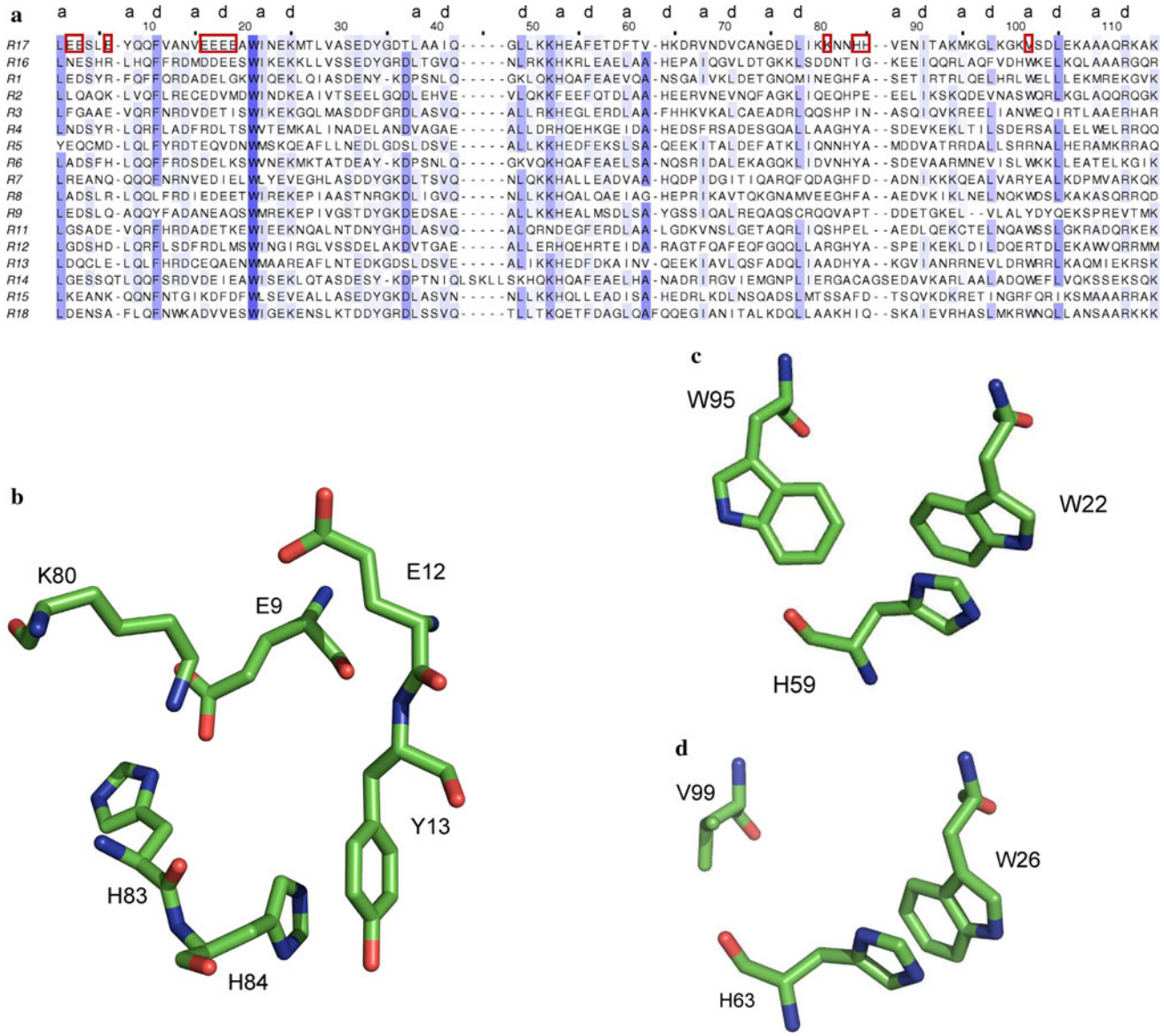

Fig. 6 **a** Sequence alignment of 17 repeats of chicken brain α spectrin (Swiss-Prot: P07751). The sequences start with the linker between two successive repeats and end right before the next linker. Conserved hydrophobic residues in the heptad pattern are indicated. Exceptional residues in R17 are marked in red. Multiple sequence alignment was accomplished by MUSCLE (Edgar 2004) in Jalview 2.6.1 (Waterhouse et al. 2009). The repeats 10 and 19 were excluded from the alignment because of major sequence diversity. **b** Interactions between the linker-region and the BC-loop in R17 according to the crystal structure (pdb-entry 1CUN). E9 forms a salt-bridge to H83, both E9 and E12 are in position to form a salt-bridge or hydrogen bond to K80 and the aromatic ring of Y13 stacks onto the imidazole ring of H84 **c**, **d** Hydrophobic interactions in the triple-helix bundle according to the crystal structure. The presence of a valine instead of the moderately conserved tryptophan in helix C renders a cavity in the hydrophobic core of the triple-helix bundle, leading to a possible destabilization of R17 (*c*) compared to R16 (*d*). The structures were displayed with PyMOL

Stability of R17

The multiple sequence alignment of 17 out of the 19 repeats of chicken brain α-spectrin (Fig. 6a) reveals three distinct features of the R17 sequence (marked red in the alignment) which might explain its reduced stability: a stretch of four consecutive glutamic acids in helix A, an unusual amount of charged residues in the linker and the BC-loop, and a tryptophan to valine substitution in helix C.

The repulsion between four subsequent negatively charged amino acids might destabilize helix A as suggested by the relaxation data (Fig. 3a–c) and the broadening of amide proton resonances observed for E21, E22 and E23. However, R17 shares this unusual feature with R16 and it is, thus, unlikely that the four glutamic acids can explain why R17 is less stable than R16.

R17 contains considerably more charged residues in the linker and the BC-loop (positions 1–7 and 81–85 in Fig. 6a, respectively) than the other 16 chicken brain α-spectrin repeats: three with negative charges in the linker and three with positive charges in the BC-loop. From the crystal structure it is evident that the opposite charges in the linker stabilize the BC-loop in R17: E9 interacts with K80 and H83, E12 might interact with K80, and the aromatic side chains of Y13, close to the linker, and H84 stack on top of each other (Fig. 6b). In comparison, there is only one salt-bridge between the linker and the BC-loop in R16 (Kusunoki et al. 2004b). The inclusion of the linker might explain why the melting point, 313 K according to CD-results, of our R17 construct is significantly higher than the previously reported 304 K (Kusunoki et al. 2004a). Motions within the BC-loop and the linker at micro- to milli-second time scale could account for line-broadened and missing amide resonances in this region.

But even with the inclusion of the linker, our R17 construct is still less thermodynamically stable compared to other single repeats like R16. The main reason for the reduced stability of R17 might be the lack of the moderately conserved tryptophan in helix C leading to fewer hydrophobic interactions in the core of the domain compared to other repeats (Kusunoki et al. 2004b). The highly conserved tryptophan in helix A interacts with a residue in a *d* position in helix B (H63 in R17) and the moderately conserved tryptophan in helix C (Pascual et al. 1997). Both tryptophans have proven to promote conformational stability in spectrin repeats (MacDonald et al. 1994; Pantazatos and MacDonald 1997). In the multiple sequence alignment of 17 chicken brain α-spectrin repeats the first tryptophan (position 21 in Fig. 6a) is 100 % conserved, whereas the second tryptophan (position 102) is conserved in 10 out of 17 repeats. The latter is either substituted by another aromatic side chain or by the large, positive side chain of arginine, whereas R17 only contains the relatively small aliphatic side chain of valine. As a result, the domain is destabilized by this substitution which introduces a cavity in the hydrophobic core between the three helices (Fig. 6c, d). The H^N-exchange study indicates that the hydrophobic core in the region of W26, F60/H63 and V99 is compact at room temperature. Even though the backbone-NH signals of W26, F60 and H63 are solvent exchanged within 1 h upon addition of D_2O, V99 is one of the 16 residues that are not completely deuterated after 8 h. E22, E24, A25 and E103 are examples of amino acids with very slow exchange rates, indicating that especially W26 is situated in a highly hydrophobic environment.

As the temperature was raised, some of the NH-, C′ and C^{α} resonances split in two or more peaks. One may interpret this splitting as a change in the conformation between the folded and the unfolded state of the repeat. Unfolding of R17 could happen in three different ways: sudden complete unfolding in an all-or-none process, local unfolding in one or more of the helices, and the break-up of the triple-helix bundle. The observation of line splitting for a limited set of residues at increasing temperatures with a simultaneous lack of a sharp transition for amide proton shifts, suggests that unfolding of R17 most likely does not follow an all-or-none process. Conformational changes at room-temperature in the BC-loop and nearby residues, like E75 (Fig. 3b) and K93 (Fig. 3a, c), could lead to local unfolding of helices B and C from the loop since higher temperatures are expected to increase the exchange rates. Still, even at 321 K no helical collapse was observed by NMR spectroscopy. However, three out of the six helical residues that experienced peak splitting upon temperature increment—L95, G97 and S100—are situated in the centre of helix C, close to V99. This indicates that this part of the helix could initiate the break-up of the tertiary structure of R17. Unfortunately, the NH-peak of V99 overlaps severely as the temperature is raised, but at 317 K its C′ and C^{α} resonances are split. Furthermore, W26 has a broadened NH-peak at 317 K. The reduced stability of the hydrophobic core of R17 has been reported in several mutagenesis studies: the mutation of the first tryptophan into phenylalanine in R16 reduced the ΔG of unfolding by 50 % (Pantazatos and MacDonald 1997), whereas the R17 W26F mutant was completely unfolded (Batey et al. 2006). Furthermore, the mutation of the second tryptophan into valine in R16 also reduced the ΔG of unfolding by 50 % (Pantazatos and MacDonald 1997). Thus, initial thermal unfolding of R17 with helix C separating from helices A and B could be consistent with the weakened interhelical interaction in the hydrophobic core around V99.

In conclusion, this study provides a view of the unfolding process of chicken-brain α-spectrin repeat 17 at an amino acid level and an explanation for the observed differences in stability between R16 and R17. Our results

suggest further comparative NMR studies of spectrin repeats which express variations in their thermodynamical and conformational stability.

Acknowledgments We are grateful to Anne Chapelle for preparation of isotopically labelled samples of the R17 domain, and to Jarl Underhaug for help with the NMRPipe-scripts for the relaxation study.

References

An XL, Zhang XH, Salomao M, Guo XH, Yang Y, Wu Y, Gratzer W, Baines AJ, Mohandas N (2006) Thermal stabilities of brain spectrin and the constituent repeats of subunits. Biochemistry 45(45):13670–13676. doi:10.1021/bi061368x

Batey S, Scott KA, Clarke J (2006) Complex folding kinetics of a multidomain protein. Biophys J 90(6):2120–2130. doi:10.1529/biophysj.105.072710

Bennett V, Gilligan DM (1993) The spectrin-based membrane skeleton and micron-scala organization of the plasma-membrane. Annu Rev Cell Biol 9:27–66

Carugo KD, Banuelos S, Saraste M (1997) Crystal structure of a calponin homology domain. Nat Struct Biol 4(3):175–179

Davis AL, Keeler J, Laue ED, Moskau D (1992) Experiments for recording pure-absorption heteronuclear correlation spectra using pulsed field gradients. J Magn Reson 98(1):207–216

de la Torre JG, Huertas ML, Carrasco B (2000) HYDRONMR: prediction of NMR relaxation of globular proteins from atomic-level structures and hydrodynamic calculations. J Magn Reson 147(1):138–146. doi:10.1006/jmre.2000.2170

Delaglio F, Grzesiek S, Vuister GW, Zhu G, Pfeifer J, Bax A (1995) NMRPipe—a multidimensional spectral processing system based on UNIX Pipes. J Biomol NMR 6(3):277–293

Diercks T, Coles M, Kessler H (1999) An efficient strategy for assignment of cross-peaks in 3D heteronuclear NOESY experiments. J Biomol NMR 15(2):177–180

Dosset P, Hus JC, Blackledge M, Marion D (2000) Efficient analysis of macromolecular rotational diffusion from heteronuclear relaxation data. J Biomol NMR 16(1):23–28

Edgar RC (2004) MUSCLE: multiple sequence alignment with high accuracy and high throughput. Nucleic Acids Res 32(5):1792–1797. doi:10.1093/nar/gkh340

Fung LWM, Lu HZ, Hjelm RP, Johnson ME (1986) Selective detection of rapid motions in spectrin by NMR. FEBS Lett 197(1–2):234–238

Fung LWM, Lu HZ, Hjelm RP, Johnson ME (1989) Quantitative detection of rapid motions in spectrin by NMR. Life Sci 44(11):735–740

Grum VL, Li DN, MacDonald RI, Mondragon A (1999) Structures of two repeats of spectrin suggest models of flexibility. Cell 98(4):523–535

Grzesiek S, Bax A (1993a) Amino-acid type determination in the sequential assignment procedure of uniformly C-13/N-15-enriched proteins. J Biomol NMR 3(2):185–204

Grzesiek S, Bax A (1993b) The importance of not saturating H_2O in protein NMR—application to sensitivity enhancement and NOE measurements. J Amer Chem Soc 115(26):12593–12594

Grzesiek S, Anglister J, Bax A (1993) Correlation of backbone amide and aliphatic side-chain resonances in C-13/N-15-enriched proteins by isotropic mixing of C-13 magnetization. J Magn Reson B 101(1):114–119

Harris RK, Becker ED, De Menezes SMC, Granger P, Hoffman RE, Zilm KW (2008) Further conventions for NMR shielding and chemical shifts (IUPAC recommendations 2008). Pure Appl Chem 80(1):59–84. doi:10.1351/pac200880010059

Kamath U, Shriver JW (1989) Characteriazation of thermotropic state changes in myosin subfragment-1 and heavy-meromyosin by UV difference spectroscopy. J Biol Chem 264(10):5586–5592

Kay LE, Torchia DA, Bax A (1989) Backbone dynamics of proteins as studied by N-15 inverse detected heteronuclear NMR-spectroscopy—application to staphylococcal nuclease. Biochemistry 28(23):8972–8979

Keller RLJ (2005) Optimizing the process of nuclear magnetic resonance spectrum analysis and computer aided resonance assignment. ETH Zürich, Zürich

Kowalski K, Merkel AL, Booker GW (2004) H-1, C-13 and N-15 resonance assignments of the third spectrin repeat of alpha-actinin-4. J Biomol NMR 29(4):533–534. doi:10.1023/b:jnmr.0000034342.20537.01

Kusunoki H, Macdonald RI, Mondragon A (2004a) Structural insights into the stability and flexibility of unusual erythroid spectrin repeats. Structure 12(4):645–656. doi:10.1016/j.str.2004.02.022

Kusunoki H, Minasov G, MacDonald RI, Mondragon A (2004b) Independent movement, dimerization and stability of tandem repeats of chicken brain alpha-spectrin. J Mol Biol 344(2):495–511. doi:10.1016/j.jmb.2004.09.019

Legardinier S, Legrand B, Raguenes-Nicol C, Bondon A, Hardy S, Tascon C, Le Rumeur E, Hubert JF (2009) A two-amino acid mutation encountered in Duchenne muscular dystrophy decreases stability of the rod domain 23 (R23) spectrin-like repeat of dystrophin. J Biol Chem 284(13):8813–8823. doi:10.1074/jbc.M805846200

Lipari G, Szabo A (1982a) Model-free approach to the interpretation of nuclear magnetic-resonance relaxation in macromolecules. 1. Theory and range of validity. J Am Chem Soc 104(17):4546–4559

Lipari G, Szabo A (1982b) Model-free approach to the interpretation of nuclear magnetic-resonance relaxation in macromolecules. 2. Analysis of experimental results. J Am Chem Soc 104(17):4559–4570

MacDonald RI, Musacchio A, Holmgren RA, Saraste M (1994) Invariant tryptophan at a shielded site promotes folding of the conformational unit of spectrin. Proc Natl Acad Sci 91(4):1299–1303

Montelione GT, Lyons BA, Emerson SD, Tashiro M (1992) An efficient triple resonance experiments using C-13 isotropic mixing for determining sequence-specific resonance assignments of isotopically-enriched proteins. J Am Chem Soc 114(27):10974–10975

Musacchio A, Noble M, Pauptit R, Wierenga R, Saraste M (1992) Crystal-structure of a src-homology-3 (SH3) domain. Nature 359(6398):851–855

Pantazatos DP, MacDonald RI (1997) Site-directed mutagenesis of either the highly conserved Trp-22 or the moderately conserved Trp-95 to a large, hydrophobic residue reduces the thermodynamic stability of a spectrin repeating unit. J Biol Chem 272(34):21052–21059

Park S, Caffrey MS, Johnson ME, Fung LWM (2003) Solution structural studies on human erythrocyte alpha-spectrin tetramerization site. J Biol Chem 278(24):21837–21844. doi:10.1074/jbc.M300617200

Parry DAD, Dixon TW, Cohen C (1992) Analysis of the 3-alpha-helix motif in the spectrin superfamily of proteins. Biophys J 61(4):858–867

Pascual J, Pfuhl M, Rivas G, Pastore A, Saraste M (1996) The spectrin repeat folds into a three-helix bundle in solution. FEBS Lett 383(3):201–207

Pascual J, Pfuhl M, Walther D, Saraste M, Nilges M (1997) Solution structure of the spectrin repeat: a left-handed antiparallel triple-helical coiled-coil. J Mol Biol 273:740–751

Sahr KE, Laurila P, Kotula L, Scarpa AL, Coupal E, Leto TL, Linnenbach AJ, Winkelmann JC, Speicher DW, Marchesi VT,

Curtis PJ, Forget BG (1990) The complete cDNA and polypeptide sequences of human erythroid alpha-spectrin. J Biol Chem 265(8):4434–4443

Sattler M, Schleucher J, Griesinger C (1999) Heteronuclear multidimensional NMR experiments for the structure determination of proteins in solution employing pulsed field gradients. Prog Nucl Magn Reson Spectrosc 34(2):93–158

Schanda P, Kupce E, Brutscher B (2005) SOFAST-HMQC experiments for recording two-dimensional heteronuclear correlation spectra of proteins within a few seconds. J Biomol NMR 33(4): 199–211. doi:10.1007/s10858-005-4425-x

Schubert M, Smalla M, Schmieder P, Oschkinat H (1999) MUSIC in triple-resonance experiments: amino acid type-selective H-1-N-15 correlations. J Magn Reson 141(1):34–43

Schubert M, Oschkinat H, Schmieder P (2001a) MUSIC and aromatic residues: Amino acid type-selective H-1-N-15 correlations, III. J Magn Reson 153(2):186–192. doi:10.1006/jmre.2001.2447

Schubert M, Oschkinat H, Schmieder P (2001b) MUSIC, selective pulses, and tuned delays: Amino acid type-selective H-1-N-15 correlations, II. J Magn Reson 148(1):61–72

Travé G, Lacombe PJ, Pfuhl M, Saraste M, Pastore A (1995) Molecular mechanism of the calcium-induced conformational change in the spectrin EF-hands. EMBO J 14(20):4922–4931

Vranken WF, Boucher W, Stevens TJ, Fogh RH, Pajon A, Llinas P, Ulrich EL, Markley JL, Ionides J, Laue ED (2005) The CCPN data model for NMR spectroscopy: development of a software pipeline. Proteins Struct Funct Bioinform 59(4):687–696. doi: 10.1002/prot.20449

Vuister GW, Bax A (1993) Quantitative J correlation—a new approach for measuring homonuclear 3-bond J(H(N)H(alpha)) coupling-constants in N-15-enriched proteins. J Am Chem Soc 115(17):7772–7777

Wang YJ, Jardetzky O (2002) Probability-based protein secondary structure identification using combined NMR chemical-shift data. Protein Sci 11(4):852–861. doi:10.1110/ps.3180102

Waterhouse AM, Procter JB, Martin DMA, Clamp M, Barton GJ (2009) Jalview Version 2-a multiple sequence alignment editor and analysis workbench. Bioinformatics 25(9):1189–1191. doi: 10.1093/bioinformatics/btp033

Weisemann R, Ruterjans H, Schwalbe H, Schleucher J, Bermel W, Griesinger C (1994) Determination of H(N), H-alpha and H(N), C′ coupling-constants in C-13, N-15-labeled proteins. J Biomol NMR 4(2):231–240

Winkelmann JC, Costa FF, Linzie BL, Forget BG (1990) Beta-spectrin in human skeletal-muscle–tissue-specific differential processing of 3′ beta-spectrin pre-messenger-RNA generates a beta-spectrin isoform with a unique carboxyl terminus. J Biol Chem 265(33):20449–20454

Wishart DS, Sykes BD, Richards FM (1991) Relationship between nuclear-magnetic-resonance chemical-shift and protein secondary structure. J Mol Biol 222(2):311–333

Wishart DS, Bigam CG, Yao J, Abildgaard F, Dyson HJ, Oldfield E, Markley JL, Sykes BD (1995) H-1, C-13 and N-15 chemical-shift referencing in biomolecular NMR. J Biomol NMR 6(2):135–140

Wüthrich K, Billeter M, Braun W (1984) Polypeptide secondary structure determination by nuclear magnetic-resonance observation of short proton proton distances. J Mol Biol 180(3):715–740

Yamazaki T, Formankay JD, Kay LE (1993) 2-Dimensional NMR experiments for correlating C-13-beta and H-1-delta/epsilon chemical-shifts of aromatic residues in C-13-labeled proteins via scalar couplings. J Am Chem Soc 115(23):11054–11055

Yan Y, Winograd E, Viel A, Cronin T, Harrison SC, Branton D (1993) Crystal-structure of the repetetive segments of spectrin. Science 262:2027–2030